

STRUCTURAL ANALYSES & EXPERIMENTAL ACTIVITIES SUPPORTING THE DESIGN OF A LIGHTWEIGHT RIGID-WALL MOBILE SHELTER

Paul V. Cavallaro*
U.S. Naval Undersea Warfare Center
Newport, RI 02481

Melvin Jee
U.S. Army Natick Soldier Research, Development and Engineering Center
Natick, MA 01760

ABSTRACT

Lightweight rigid-wall shelters used in mobile military operations are constructed of sandwich panels comprised of thin face sheets and thick, ultra light core materials to minimize weight and maximize structural integrity. However, such lightweight construction comes at a cost, often impacting the design and manufacturing of critical joints connecting the sandwich panels in a box-like assembly. Furthermore, joint stiffnesses are often difficult to characterize and their finite values significantly influence panel deflections and rotations. Although mobile rigid wall shelters must be certified for several transport loading environments, this effort, combines experimental and analytical approaches at material and sub-structural levels to (1) generate accurate modeling methods, (2) validate material- and sub-structural models and (3) virtually evaluate the shelter's structural performance while minimizing costly physical testing. Material-level tests focused on the mechanics of the assembled constituents forming the sandwich panel and the benchmarking of appropriate finite elements to predict displacements, stresses and strains. The sub-structural level tests focused on loading a structurally representative shelter section to determine the joint behaviors and stiffnesses for model benchmarking purposes. Finally, a complete rigid-wall shelter model was constructed for evaluating future static and dynamic load cases as required for certification.

1. INTRODUCTION

A lightweight rigid wall shelter was constructed for mounting on various military vehicles such as the High Mobility Multi-Purpose Wheeled Vehicle (HMMWV) as shown in Fig. (1). The shelter was primarily constructed of thin aluminum face sheets (skins) adhesively bonded to a relatively thick paper honeycomb core forming a sandwich panel construction (SPC) interconnected with various aluminum extrusions, weldments, mechanical fasteners and adhesive bonds. Structural advantages result from the decoupling of bending and shear behaviors between face sheet and core materials. That is, the bending stiffness is materially dependent upon the face sheets while the shear stiffness is materially dependent upon the core. No

appreciable bending strain energies develop in the core and, likewise, no appreciable shear strain energies develop in the face sheets. The decoupling of these behaviors enables the designer to achieve a level of tailorability unmatched by homogeneous materials but analogous to fiber reinforced laminates.



Fig. 1 Lightweight rigid-wall shelter shown mounted on a HMMWV.

The face sheets were 0.025" thick 6061-T6 aluminum except in the wheel well region where the face sheets were 0.015" thick 2024-T4 aluminum. Strength properties for these alloys^[1] are shown in Table (1). Hexcel® WR-II Kraft®-coated paper honeycomb core^[2] was used. This grade had a 3/8" cell size and a 2.5 lbs/ft³ weight density. Compression and transverse shear properties are shown in Table (2). The face sheets and core were bonded together using a structural film adhesive.

Table 1 Strength properties of aluminum face sheets.

Aluminum Alloys	Yield Stress (psi)	Ultimate Stress (psi)
2024-T4	45,000	68,000
6061-T6	40,000	47,000

Table 2 Properties of 1.210 inch thick WR II honeycomb.

WR II Honeycomb Core	Compression Properties (psi)			Transverse Shear Properties (psi)			
	Bare Strength	Stabilized Strength	Modulus	Across Ribbon Direction Strength	Ribbon Direction Modulus	Along Ribbon Direction Strength	Modulus
3/8" cell, 2.5 lb/ft ³	260	340	33,000	141	13,000	83	7,000

Two primary sandwich panels, folded into 3 planar sections (one panel formed the floor, front end wall and roof and the second panel formed the road side wall, door end wall and curb side wall), generally comprised the shelter. This enabled the panels to be aligned to net shape for subsequent joining using mechanical fasteners, closeout extrusions and weldments forming the closed box configuration. Using two primary sandwich panels reduced the number of joints and allowed for ease in manufacture.

A critical step enabling rapid shelter development was the integration of experimental validation tests with analytical

methods. A test plan was developed to characterize load sharing mechanisms, panel shear and flexure stiffnesses, deflections and stress states at both the material and structural levels.

2. MATERIAL LEVEL TESTING

The material level tests focused on the mechanics of an adhesively bonded aluminum/honeycomb sandwich panel subjected to flexure loads. Four-point flexure tests were performed on six 20" long by 4" wide by 1.26" thick sandwich beams as shown in Fig. (2). Four-point rather than three-point loading was selected to mitigate failures by localized core crushing prior to the onset of face sheet yielding and to provide a gage section region subjected to constant bending stress with no transverse shear stresses.

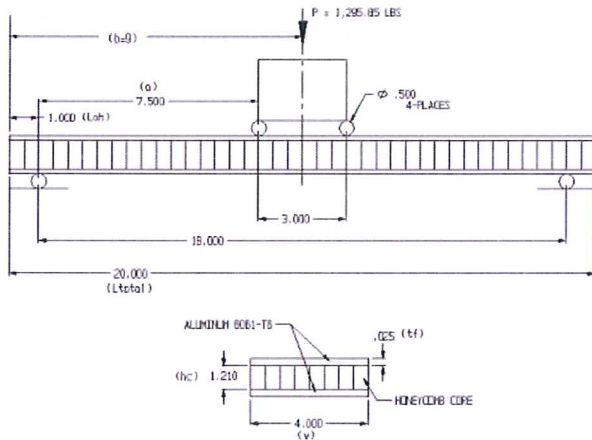


Fig. 2 Four-point flexure test specimen.

The honeycomb ribbon direction was oriented along the longitudinal axis of the beams. Uniaxial strain gages were adhered to the centers of both face sheets to avoid localized effects in the vicinity of the load points, keeping within the region of constant maximum moment. The sandwich construction represented a relatively complex assemblage of structural materials in which a variety of failure modes were possible, including (1) core crushing, (2) core crimping (shear), (3) face sheet/core delamination, (4) intra-cell buckling (dimpling) and (5) face sheet fracture. However, transverse shearing of the honeycomb core was the observed failure mode for each panel tested. Failures occurred at both the load and support points. The mid-span deflections, peak face sheet strains and applied loads are summarized in Table (3). Correlation of the FEA results to the four point bend test data validated the ability of the sandwich element model to accurately predict the: (1) distribution of bending stresses within the face sheets, (2) transverse shear stresses in the honeycomb core, (3) interlaminar shear stresses within the adhesive layers, (4) bending and transverse shearing components of the total deflection, (5) load required to fail the honeycomb core in shear, (6) load required to fail the

adhesive layer between the honeycomb core and face sheets and (7) load required to initiate yielding of the face sheets.

Table 3 Results of material level four-point flexure tests.

Spec. #	Total Load (lbs)	Maximum Moment (in-lbs)	Maximum Shear Force (lbs)	Tensile Face Sheet Strain (in/in)	Compressive Face Sheet Strain (in/in)	Maximum Face Sheet Axial Stress (psi)	Maximum Honeycomb Transverse Shear Stress (psi)	Mid-Span Deflection (in)
1	1,021.06	3,828.98	510.53	3,176.75	-3,135.88	31,627.11	103.33	0.251
2	1,038.57	3,894.64	519.29	3,094.18	-3,049.98	32,169.48	105.10	0.250
3	955.37	3,582.64	477.69	2,880.68	-2,713.87	29,592.37	96.68	0.252
4	857.66	3,216.23	428.83	2,509.54	-2,434.48	26,565.83	86.80	0.194
5	971.14	3,641.78	485.57	2,874.00	-2,876.51	30,080.85	98.28	0.220
6	1,052.46	3,946.73	526.23	3,236.80	-3,062.49	32,599.72	106.51	0.237

3. MECHANICS OF SANDWICH PANELS - EFFECT OF CORE TRANSVERSE SHEAR MODULI

The design of a SPC for structural applications is analogous to that of I-beams, where the face sheets (flanges) are designed to support flexure loads while the core (web) supports the transverse shear loads^[3]. An extension of Allen's^[4] analysis for SPC consisting of relatively thin, yet stiff, face sheets and relatively thick, but compliant, core layer was performed to investigate the effects of the honeycomb core's transverse shear modulus on the deflection response of the four-point bend specimens.

Assuming linear elasticity and symmetric face sheets, small deflection theory was invoked whereby the mid-plane was assumed to be coincident with the neutral surface. The neutral surface, by definition, is a surface having no bending stresses or deformations due to bending. In-plane axial stresses acting on the neutral surface are referred to as membrane stresses. Since SPC's by design have considerable bending stiffness and, if membrane stresses exist, the coupled effects between bending and membrane stresses (analogous to load stiffening of beams) must be considered. This results in the need for a large deflection (nonlinear) solution. The need for large deflection solutions of homogeneous plates may be necessary even for the case of transverse loads alone. However, for SPC's conforming to the following restrictions, small deflection theory should be sufficient.

1. The SPC is constructed with a relatively thick, compliant core layer (i.e.; negligible elastic moduli but appreciable transverse shear moduli).
2. Face sheets are symmetric in material and thickness.
3. The SPC is subjected to only transverse loads.
4. No membrane stresses exist on the neutral surface.

The following analysis invokes linear elasticity (small deformation theory) and describes the mid-span deflection, δ , face sheet longitudinal stress, σ_{xx} , face sheet longitudinal strain, ϵ_{xx} , and core transverse shear stress, τ_{xz} , as functions of applied load. From Euler Beam Theory (EBT)^[5], the face sheet longitudinal stress, σ_{xx} , from flexure loading is a linear function of the bending moment, M , distance, y , from neutral surface to

point of interest, and area moment of inertia, I , for a sandwich beam having total thickness t_{total} :

$$\sigma_{xx} = \frac{My}{I} \quad (1)$$

where: $-t_{total}/2 \leq y \leq +t_{total}/2$

The maximum face sheet longitudinal stress, σ_{max} , is obtained at locations of maximum moment and distance furthest from the neutral axis. For the case of four-point flexure loading of symmetric sandwich beams, σ_{max} becomes:

$$\sigma_{max} = \frac{\left(P_{max} \frac{a}{2} \right) \left(\frac{t_c + 2t_f}{2} \right)}{\frac{w}{12} (t_c + 2t_f)^3} \quad (2)$$

where: t_c = core thickness,
 t_f = face sheet thickness
 w = width of cross section
 a = distance between load & support point
 P_{max} = maximum applied machine load

For an isotropic material, the face sheet longitudinal strain, ϵ_{max} , corresponding to σ_{max} is obtained by assuming a uniaxial stress field such that:

$$\epsilon_{max} = \frac{\sigma_{max}}{E_{xx}} \quad (3)$$

where: E_{xx} = Young's Modulus in x-direction

Castigliano's Second Theorem was used to derive an expression for maximum lateral deflection based on considering the combined strain energies due to bending of the face sheets and transverse shearing of the honeycomb core. This is equivalent to a Timoshenko beam solution in which the effect of transverse shear deformation on lateral deflection is included^[6]. The maximum deflection, δ_{total} , is the sum of the mid-span contributions from the face sheet bending deformations and the core transverse shearing deformation:

$$\delta_{total} = \frac{Pa(3b^2 - a^2)}{E_f w [(t_c + 2t_f)^3 - t_c^3]} + \frac{3Pa}{5G_c w t_c} \quad (4)$$

where: b = distance between load points
 G_c = core transverse shear modulus

The flexural rigidity, D_s , of the sandwich is computed using the parallel axis theorem and Young's Modulus for each layer as:

$$D_s = \frac{E_f w t_f^3}{6} + \frac{E_f w t_f}{2} d^2 + \frac{E_c w}{12} t_c^3 \quad (5)$$

where: d = distance between face sheet mid-planes

The transverse shear stress, τ_{xzc} , in the core as a function of the through-thickness variable y_c is then given as:

$$\tau_{xzc}(y_c) = \frac{V}{2D_s} \left[E_f t_f d + E_c \left(\frac{t_c^2}{4} - y_c^2 \right) \right] \quad (6)$$

where: V = shearing force
 $-t_c/2 \leq y_c \leq +t_c/2$

If $E_c \ll E_f$, then the transverse shear stress of the honeycomb core is constant through the thickness as the product involving E_c becomes negligible. The transverse shear stress distribution in either face sheet (both face sheets assumed to be of equal thickness and material) as a function of the through-thickness variable y_f is:

$$\tau_{xzf}(y_f) = \frac{V}{D_s} \left[\frac{(t_c^2 + 4t_c t_f + t_f^2 - 4y_f^2) E_f}{8} \right] \quad (7)$$

where: $0 \leq y_f \leq t_f$

The maximum value of τ_{xyf} occurs at the inner surface of the face sheet. To determine the applied load required to initiate yielding of the face sheets, the yield stress of aluminum 6061-T6 ($\sigma_{yield} = 40,000$ psi) was substituted into Eq. (1) and solved for P_{max} upon which $P_{yield} = P_{max}$.

$$P_{yield} = 1,295.85 \text{ lbs.}$$

The corresponding deflection terms, axial face sheet strain [$E_f = 10 \times 10^6$ psi] and honeycomb transverse shear stress [for WR-II-3/8-2.5 honeycomb along the ribbon direction, $G_c = 13,000$ psi and $\tau_{xzc, allowable} = 141$ psi (thickness correction factor included on transverse shear strength)] at yield are:

$$\begin{aligned} \delta_{shear} &= 0.093 \text{ in}, & \delta_{bend} &= 0.198 \text{ in} & \delta_{total} &= 0.291 \text{ in} \\ \epsilon_{yield} &= 0.004 \text{ in/in}, & \tau_{xzc} &= 131 \text{ psi} \end{aligned}$$

The transverse shearing deformation contributed 32% toward the total mid-span deflection. The above strain represents the magnitude of strain in both the tensile (lower) and compressive (upper) face sheets since the sandwich is symmetric and linear elasticity (small deformation) is assumed. The continuity of τ_{xz} across the face sheet/core interface is checked by solving (7) at $y_f = 0$ and comparing to the value of τ_{xyc} .

$$\tau_{xzf} = 131 \text{ psi}$$

The effect of core transverse shear stiffness, G_c , on the midpoint deflection is shown in Fig. (3). Note that δ_{bend} equals the difference between the two curves shown.

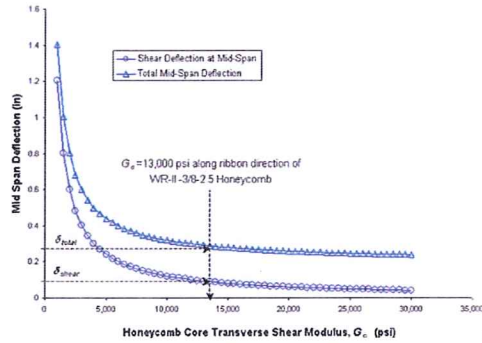


Fig. 3 Effect of honeycomb core transverse shear modulus, G_c , on mid-span deflections.

The NISA^[7] finite element program was used to model the four-point bend test specimen. Two models were generated using namely the sandwich element (type-33) and the solid composite element (type-7). The sandwich element was an 8-noded laminated shell element that supported membrane-bending coupling and transverse shear deformations. Each node had 6 degrees of freedom (DOF's), 3 translations (u_1 , u_2 and u_3) and 3 rotations (α_1 , α_2 , and α_3). However, the rotational DOF normal to the element surface, α_3 , commonly referred to as the drilling DOF, possessed no rotational stiffness. This element was developed for thick shells with two or more face sheets and one or more cores. Figure (4) shows the stress components for a general 3-D laminated composite.

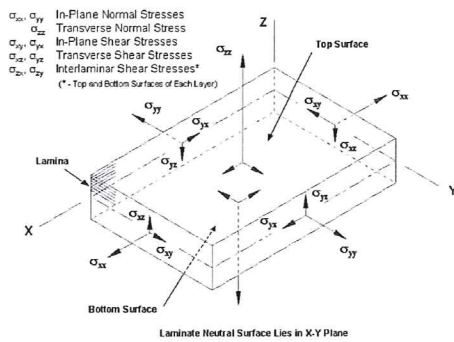


Fig. 4 General 3-D stress components for laminated composites.

The face sheets were restricted to states of plane stress (σ_{xx} , σ_{yy} , and σ_{xy}) and the core supported only transverse shear stresses (σ_{xz} and σ_{yz}). At the interface between the face sheets and the honeycomb core, the interlaminar shear stresses σ_{zx} and σ_{zy} were of particular interest. These stresses represented the in-plane shear stresses within the adhesive layer and, when compared to the allowable shear strength of the adhesive, can be used to predict adhesive shear failures. The solid composite element was a laminated brick element formulated using general 3-D states of stress (σ_{xx} , σ_{yy} , σ_{zz} , σ_{xy} , σ_{xz} , and σ_{yz}) with each node having 3 translational DOF's only. The layers of both the sandwich element and the composite solid element were assumed

perfectly bonded. Although the sandwich element did not support through-thickness deformations, which were expected to be negligible for global shelter models, it was considered significantly more computationally efficient than the solid composite element. Use of the solid composite element for a full shelter model would not be practical due to the mesh refinement required. The solid composite element was preferred in localized models where 3-dimensional stress states and through-thickness deformations were prevalent such as in joints, weldments, adhesive bonds, and fastener regions.

Displacement and stress results of the sandwich element model subjected to a total load of 1,295.85 lbs are shown in the contour plots of Figs. (5-7). At maximum load, the total displacement of 0.278 in. occurred at the mid-span and varied by only 4.5% of the analytical solution provided by Equation (4). The magnitudes of the maximum axial stress, σ_{xx} , in the tensile and compressive face sheets were identically equal to 40,400 psi, which varied by only 1.0% of Equation (2). The maximum transverse shear stress, σ_{xz} , in the honeycomb core, remote from localized effects of the load points, was 138.0 psi, which varied by 5.4% of the predicted value from Equation (6).

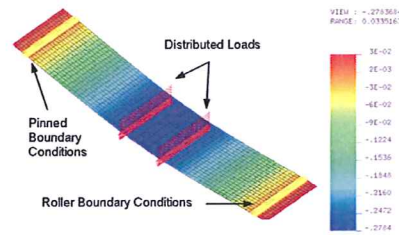


Fig. 5 Transverse displacement contour plot.

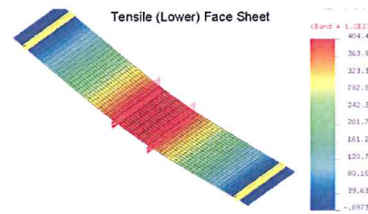


Fig. 6 Axial stress, σ_{xx} , plot for the lower face sheet.

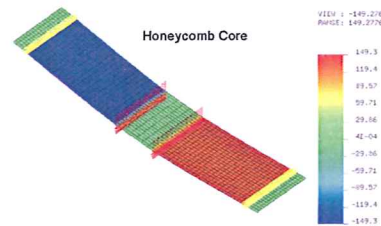


Fig. 7 Transverse shear stress, σ_{xz} , plot in the honeycomb.

The solid composite element model shown in Fig. (8) captured the through-thickness deformations at the load and support points. For the same maximum load used in the

sandwich model and closed form solution, the maximum displacement of the composite solid element model was 0.282 in. at the mid-span. However, this model did not include the effects of plasticity (stress softening) due to localized yielding of the compressive face sheet, which was evident in the tests. Post-test inspections revealed that the permanent indentations made at either the load or support points ranged in depth up to 0.06 in. The maximum axial stresses, σ_{x3} in the tensile and compressive face sheets were 40,290 psi and -40,080 psi, respectively. The maximum transverse shear stress, σ_{xz} in the honeycomb core was 141.1 psi.

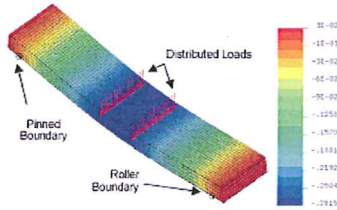


Fig. 8 Vertical displacement plot from the composite solid element model at 1,295.85 lb total load.

A comparison of mid-span deflections from the closed form solution, finite element models and experimental tests is shown in Fig. (9). The maximum load used in the closed form and finite element solutions was used to normalize the experimental deflections.

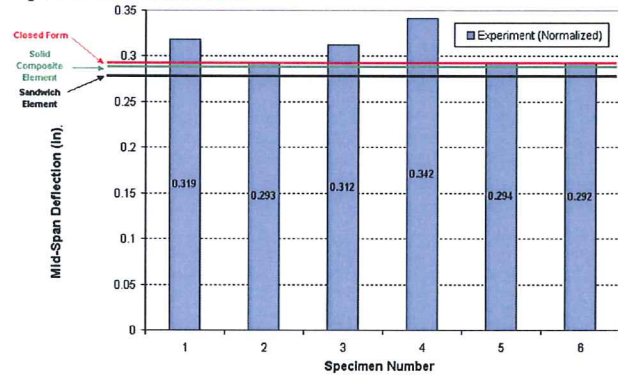


Fig. 9 Comparison of mid-span deflections.

The experimental deflections were expected to slightly exceed those predicted by the closed form and finite element methods because localized indentations of the tests and solid composite element model at the load and support points could not be simulated in the closed form solution and sandwich element model. The closed form and FEA solutions were based on linear elasticity and did not include geometric or material nonlinearities due to large deformations, plasticity, etc. The material level tests and subsequent modeling verified the significance of incorporating a shear deformable analysis method for developing the shelter. Both the sandwich and solid composite elements were successfully benchmarked for use in full shelter models provided that limitations of linear elasticity were not exceeded.

5. SUB-STRUCTURAL TESTING

The test specimen shown in Figs. (10-11), along with its restraints and four-point loading arrangement, was designed to generate flexure stresses along the shelter's hoop direction since flexure is generally the dominant mode of loading. It represented one lateral half of the shelter without the forward and rear walls.

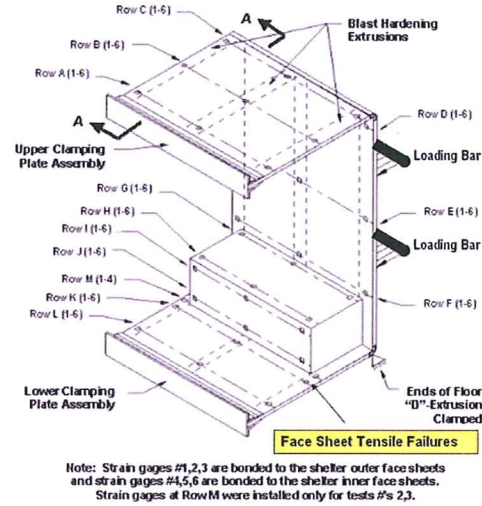


Fig. 10 Shelter section test and strain gage map.

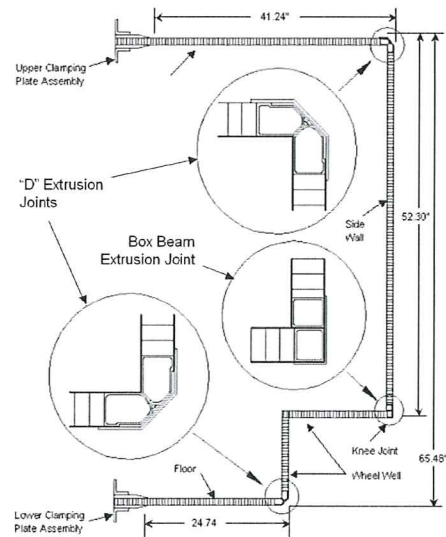


Fig. 11 Section view of representative shelter test.

The honeycomb ribbon direction was oriented parallel to the shelter hoop axis. As with the beam tests, four-point rather than three-point loading was selected to mitigate failures by localized core crushing prior to face sheet yielding. Two clamped restraints, located at each end of the floor "D"-extrusion (fore and aft of the wheel well), were necessary for generating substantial flexure stresses at the side wall/wheel well interface. Absent these clamped restraints, analysis demonstrated that: (1) flexure stresses within the side wall/wheel well region were

minimal and (2) the floor panel would fail by excessive bending deflections, which were not prevalent in certification tests because the floor contacts the vehicle's cargo area floor. The edges of the floor and roof panels were bolted to the test frame with clamping plates to provide near rigid boundary conditions. Using a test frame and hydraulic actuator, two line loads were quasi-statically applied to the side wall using the loading bars as shown in Fig. (10). The section was oriented in the test frame so that the side wall was positioned horizontally. A spherical bearing connected the loading assembly to the test frame. Since the bearing was not capable of resisting torques or bending moments, the loads applied along the two load bars were equal. Stiffness of the overall loading assembly prevented deformations of the bars along their lengths. Therefore, all points of the side wall in contact with a specific loading bar deflected the same amount as that particular load bar. However, this does not infer that deflections under both load bars were equal. A preliminary FEA model was used to identify locations for positioning up to 76 strain gages. Strain gages were bonded on the inner and outer face sheet surfaces as shown in Fig. (10). Strain gages 1 & 2 were located at the forward end of the test section, 3 & 4 were located at the middle of the test section and 5 & 6 were located at the aft end of the test section. Strain gages 1, 2 and 3 were located on the outer face sheets and 4, 5 and 6 were located on the inner face sheet surfaces. All gages were uniaxial and oriented along the shelter hoop direction. The center deflections of the side wall and roof panels were recorded using linear variable displacement transducers (LVDT's). Results of the three section tests are shown in the deflection, joint rotation and strain gage plots of Figs. (12-14). Generally noted, behavior was linear with respect to load. All strain gage rows except A and H demonstrated bending dominance. Rows A and H were subjected to appreciable membrane strains in comparison to their bending strains. The presence of membrane strains indicated load stiffening effects that introduced geometric nonlinearities at approximately 5,000 lbs.

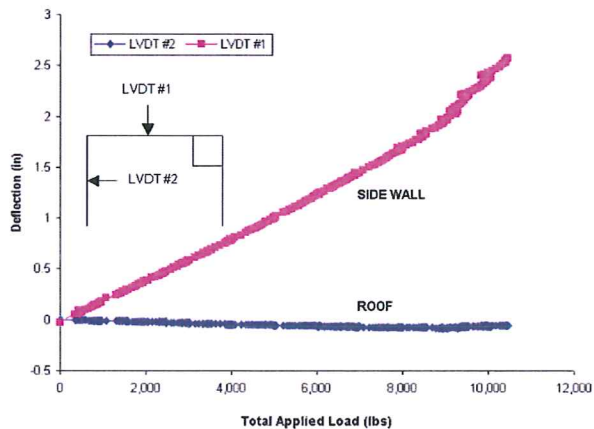


Fig. 12 Displacement vs. load for section test #3.

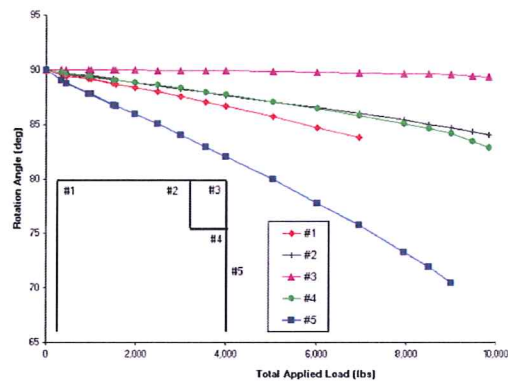


Fig. 13 Plot of rotation angles vs. load for test #3.

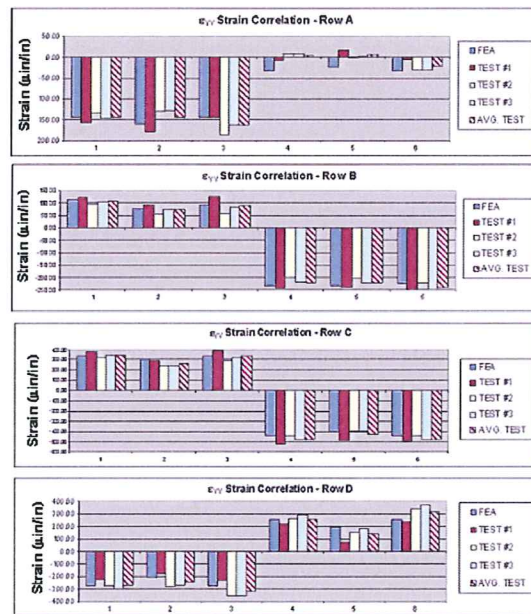


Fig. 14 Example comparisons of experimental and FEA ϵ_{yy} strains for rows A-D.

The first section test included 72 strain gages located in rows A through L. The maximum applied load was 9,935 lbs. Strains at rows D and F were mostly dominated by bending but, by contrast, were less than 25% of Row E. This suggested that the "D"-extrusion joints along the upper and lower side wall edges transferred less moment than expected for rigid connections. This counter intuitive observation rendered the restraining effects of these joints to be rotationally limited. That is, the "D"-extrusion joints behaved closer as pinned rather than rigid connections. The rotational stiffness at the wheel well-to-floor joint was comparable to those of the side wall/roof and side wall/wheel well joints. Displacement readings from the roof and side wall LVDT's at maximum load were 2.493" inward and 0.104" outward, respectively. A localized tensile fracture through the floor inner face sheet and the blast hoop stiffener occurred inches forward of the wheel well region as shown in Fig. (10). Although some plastic deformation of the side wall was evident, there were no face sheet/core delaminations or fractures of the honeycomb core.

Instrumentation of the second test section was modified to include additional strain gages located at row M. The maximum load during the second test was 10,422 lbs. with a tensile fracture of the inner face sheet and hoop stiffener occurring directly through strain gage M3. This failure location was symmetrically opposite that of the first test. Strains were consistent with those obtained from the first test. The maximum roof and side wall displacements were 2.859" inward and 0.051" outward, respectively. Plastic deformations were evident in the "D"-extrusions of the roof/side wall joint, side wall and floor panels. There were, however, no delaminations between the face sheets and honeycomb core or fractures of the honeycomb.

Two modifications were made to the testing of the third section specimen. Dial indicators were used to measure relative motions at the five locations shown in Fig. (13) so that changes in joint angles could be calculated. The maximum load was 10,441 lbs. with a tensile failure of the inner face sheet and hoop stiffener occurring adjacent to strain gage M3. Deflection readings for the LVDT's were 2.574" inward for the side wall and 0.058" outward for the roof. Post-test inspection revealed no delaminations between the face sheets and honeycomb core and no core fractures. Joint and panel rotation angles were plotted in Fig. (13) as a function of load. The maximum-recorded change in joint angle was -6.3°, which occurred at the roof/side wall joint at 6,950 lbs. This was not, however, the maximum load but the load at which the dial indicator slipped and no further measurements at this location were possible. A linear extrapolation predicted that the roof/side wall joint rotated by -7.0° had the dial indicator remained in the proper position. The floor panel rotation was 19.6° at maximum load.

Failure modes for each of the 3 section tests were identical, occurring at symmetric positions across the floor. Failure loads varied by less than 5% of their average. Strain distributions were repeatable. Deflection readings from the roof and sidewall LVDT's were linear up to the onset of yielding at the fracture regions. Strain results of each section test counter intuitively revealed that the "D"-extrusion joints were compliant rather than rigid as originally anticipated. The observed limited rotational resistance was expected to have an impact on the strain and deflection behavior of the full shelter.

A linear elastic model of the sub-structural test specimen of Fig. (10) was developed to simulate the test behavior and to match the strain gage and LVDT deflection results. The model included 2nd-ordered sandwich elements for the panels, beam elements for the extrusions and spring elements for calibrating the joint rotational stiffnesses. A nominal 10,000 lb. total load was applied and the joint rotational stiffnesses were adjusted until the model matched the experimental strain, deflection and joint rotation results.

Correlation of the experimental versus FEA strains is shown in the bar charts of Fig. (14). The LVDT and FEA deflection results were tabulated in Table (4). The joint rotational stiffnesses, K_{ROT} , used in the FEA model are shown in Table (5). These stiffnesses provided the necessary calibration to best match strains and deflections between the model and tests.

Table 4 Experimental & FEA deflections.

Deflection Results At 5,000 lb. Total Load (Negative indicates outward)		
	Sidewall	Roof
FEA	0.878	-0.121
Test #1	1.009	-0.079
Test #2	0.809	-0.105
Test #3	1.014	0.055

However, comparisons between experimental and FEA results were shown for a load of up to 5,000 lbs. Beyond this load, the nonlinearities observed at strain gage rows A and H could not be reflected by the linear elastic model. The bar charts of experimental and predicted strains shown in Fig. (14) generally demonstrated a high level of correlation.

Table 5 Section test joint rotational stiffnesses.

Joint Location Description	K_{ROT} (In-lb/rad)
Roof To Side Wall	2,500
Side Wall To Wheel Well	2,500
Wheel Well To Floor	2,500
Side Wall To Floor	5,000
Wheel Well Horizontal To Floor	2,500
Side Wall To Vertical Wheel Well	5,000
Floor To Wheel Well Fore & Aft	2,500
Clamped Edges	55,000

5. SHELTER MODEL FOR MODAL & DYNAMIC CASES

A complete structural model of the shelter was developed as shown in Figs. (15-16). This model included all sandwich panel sections, extrusions, joint rotational stiffnesses, and rigid boundary conditions that simulated the shelter-to-vehicle mounting attachments.

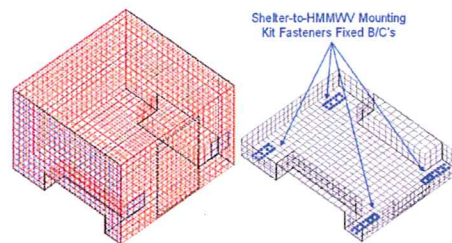


Fig. 15 Complete shelter FEA model.

Each of these was required for predicting the response of the full shelter to various loading events when mounted to the HMMWV. Rigid link elements represented the hinges and striker mechanisms connecting the door panel to the door end wall. The demarc panel elements were connected to the sandwich elements and closeout extrusions by using rigid links. The second ordered sandwich and linear beam elements used in the section model were used for the full shelter model.

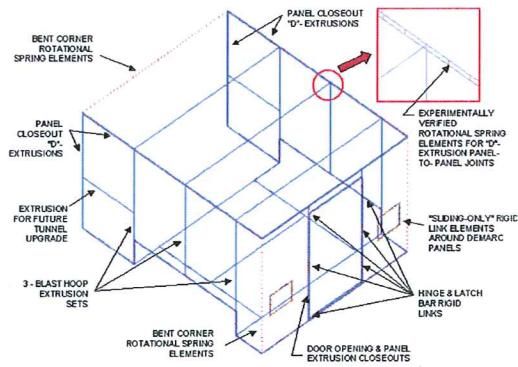


Fig. 16 Description of beam, spring and rigid link elements.

6. MODAL & DAMPING ANALYSES

For dynamic events, the time-based equations of motion shown in equation (8) included effects due to damping. The damped behavior of the shelter was determined by conducting an eigenvalue analysis that established natural frequencies of vibration, f_i , and corresponding mode shapes so that proper damping values could be established.

$$[M]\ddot{X} + [C]\dot{X} + [K]X = \{f(t)\} \quad (8)$$

where: $[M]$ = global mass matrix

$[C]$ = damping matrix

$\{f(t)\}$ = vector of nodal forces

$[K]$ = global stiffness matrix

X = vector of nodal displacements

\dot{X} = vector of nodal velocities

\ddot{X} = vector of nodal accelerations

Rayleigh damping^[8] (also known as proportional damping) was assumed in accordance with equation (9), which reflected contributions from both mass-based damping, α , and stiffness-based damping, β . In general, stiffness-based damping results from hysteretic effects observed during cyclic loading of elastic materials. Additional sources of structural damping were expected from mechanically fastened joints and face sheet/honeycomb core adhesive layers. Mass-based damping affects the dynamic response at lower frequencies while structural-based damping affects dynamic response at higher frequencies. A recommended critical damping ratio, ζ , of 5% was used for all flexure modes.

$$[C] = \alpha[M] + \beta[K] \quad (9)$$

$$\text{where: } \alpha = \frac{2\omega_i\omega_j}{\omega_j^2 - \omega_i^2} (\omega_j\zeta_i - \omega_i\zeta_j) \quad (10)$$

$$\beta = \frac{2}{\omega_j^2 - \omega_i^2} (\omega_j\zeta_j - \omega_i\zeta_i) \quad (11)$$

$$\omega_i = 2\pi f_i, \quad \zeta = \frac{C}{C_c}, \quad \zeta_i = \zeta_j = 0.05 \quad (12)$$

The eigenvalue analysis was performed using the Lanczos Method^[8] with an upper cut-off frequency, f_c , of 100 Hz. The computed mode shapes (eigenvectors) were flexure dominant with symmetric and anti-symmetric deformations. The fundamental natural frequency, f_1 , was a symmetric flexure mode of the roof at 30.45 cycles/sec (Hz). Plots of the first 4 mode shapes are shown in Fig. (17). Using $\omega_1 = 191.32$ rad/sec and $\omega_2 = 227.33$ rad/sec corresponding to f_1 and f_2 , respectively, α and β were computed as $\alpha = 10.389$, $\beta = 2.389 \times 10^{-4}$.

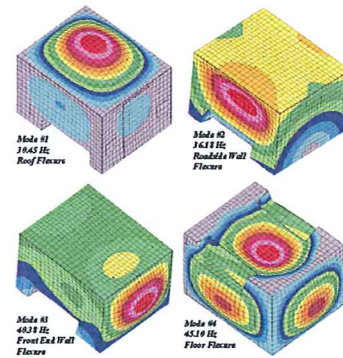


Fig. 17 Modal analysis results of first four mode shapes.

7. CONCLUSION

A modeling approach, incorporating minimal multi-level testing, was described and demonstrated for validating the design of a lightweight, mobile military shelter manufactured using sandwich panel construction (SPC) methods. This approach provided a rapid, cost-efficient alternative to the traditional "build-test-build" method. The end product of the current work is a validated, full-featured shelter model.

8. REFERENCES

1. American Society of Metals, "Metals Handbook", 1985.
2. Hexcel Corporation, "Mechanical Properties of Hexcel Honeycomb Materials", TSB #120, 1992.
3. Vinson, J.R., "The Behavior of Sandwich Structures of Isotropic and Composite Materials", Technomic Pub, 1999.
4. Allen, H. G., "Analysis and Design of Structural Sandwich Panels", Pergamon Press, Oxford, 1969.
5. Ugral, A.C., Fenster, S.K., "Advanced Strength and Applied Elasticity", Elsevier, 1977.
6. Timoshenko, S., "Strength of Materials", Nostrand 1953.
7. NISA, Ver. 11.0, Engineering Mechanics Research Corporation, Troy, MI.
8. Bathe, K.J., "Finite Element Procedures in Engineering Analysis", Prentice-Hall, Englewood Cliffs, NJ, 1982.

